JOURNAL OF MAGNETIC RESONANCE **135,** 487–499 (1998)
ARTICLE NO. MN981602

Measurement of Cross Correlation between Dipolar Coupling and Chemical Shift Anisotropy in the Spin Relaxation of ^{13}C, ^{15}N-Labeled Proteins

Ranajeet Ghose,*[,1] Kai Huang,*[,2] and James H. Prestegard†[,3]

*Department of Chemistry, Yale University, New Haven, Connecticut 06520; and †Complex Carbohydrate Research Center, University of Georgia, Athens, Georgia 30602-4712

Received March 18, 1998; revised August 11, 1998

We present a simple method for extracting interference effects between chemical shift anisotropy (CSA) and dipolar coupling from spin relaxation measurements in macromolecules, and we apply this method to extracting cross-correlation rates involving interference of amide ^{15}N CSA and ^{15}N–^{1}H dipolar coupling and interference of carbonyl $^{13}C'$ CSA and ^{15}N–$^{13}C'$ dipolar coupling, in a small protein. A theoretical basis for the interpretation of these rates is presented. While it proves difficult to quantitatively separate the structural and dynamic contributions to these cross-correlation rates in the presence of anisotropic overall tumbling and a nonaxially symmetric chemical shift tensor, some useful qualitative correlations of data with protein structure can be seen when simplifying assumptions are made.

Key Words: **chemical shift anisotropy; dipolar coupling; interference effects; carbonyl relaxation; secondary structure.**

INTRODUCTION

The fact that the interference between chemical shift anisotropy (CSA) and dipolar coupling causes the two lines of scalar-coupled doublets to have different linewidths (*1*) is well known. The interference effects also show up in cross-correlation corrections to various spin relaxation rates that are easily measured in solution, and the fact that these effects are a useful source of structural and dynamic information is being increasingly appreciated. With sufficient measurements it is in principle possible, although in practice difficult, to separate dynamic and structural factors. In this paper we provide a simple method for measuring interference effects between CSA and dipolar coupling in a scalar-coupled two-spin system, and present a theoretical basis for their interpretation.

Structural information arises from an ability to monitor the projection of the anisotropic part of the chemical shift tensor onto various bonds connecting spin $\frac{1}{2}$ nuclei. Several authors have been able to measure the CSA projections for nuclei in sites along the protein backbone, which include amide ^{15}N (*2*), amide ^{1}H (*3, 4*) and $^{13}C_{\alpha}$ (*5*), in solution. The CSA projections of the nuclei in the $^{13}C_{\alpha}$ sites have been shown to correlate extremely well with secondary structure, and those in the amide ^{1}H sites show a strong correlation with hydrogen-bond strength (*3, 4*). The CSA of the $^{13}C'$ (carbonyl carbon), which is quite substantial, is also expected to be very sensitive to local structural effects. There have been some experimental (*6–9*) and theoretical studies (*6, 10*) on related systems indicating this fact. Dynamic information arises in a manner similar to its appearance in autorelaxation rates, but correlation time relates to the way in which two interaction vectors follow one another during reorientation. Hence, measurements can complement normal spin relaxation measurements. Aside from this potential complementarity, there has also been a renewed interest in more conventional studies of the relaxation behavior of the $^{13}C'$ in proteins over the past year or so. These studies, even without cross-correlation consideration, provide insight into the dynamics of the protein backbone (*11–15*) and complement the information obtained from amide ^{15}N relaxation studies.

The method for measuring CSA–dipole cross-correlation effects presented in this paper is based on that proposed by Tjandra and Bax (*2*). Our modification simplifies the dependence of the signal intensity on the relaxation delay. We apply this method to extract the cross-correlation rates between amide ^{15}N–^{1}H and the amide ^{15}N CSA in a ^{15}N-labeled protein, a fragment of the chaperon protein DnaJ (*28*). This is followed by the application to a ^{13}C, ^{15}N-enriched form of the same protein, to extract cross-correlation rates between $^{13}C'$ CSA and $^{15}N(i+1)$–$^{13}C'(i)$ dipolar coupling. We also present a preliminary analysis of these rates in structural and dynamic terms, pointing out the difficulties one faces in the analysis when the overall tumbling of the protein is anisotropic.

THEORY

The two I spin lines of an antiphase doublet for a scalar-coupled two spin-$\frac{1}{2}$ (I, S) system may be represented as $I^{\pm}$ =

[1] Present address : Section de Chimie, Université de Lausanne, BCH, 1015 Lausanne, Switzerland.

[2] Present address: Laboratory of Chemical Physics, National Institute of Diabetes and Digestive and Kidney Diseases, National Institutes of Health, Bethedsa, MD 20892-0520.

[3] To whom correspondence should be addressed.

1090-7807/98 $25.00

$\frac{1}{2}(2I_yS_z \pm I_y)$. In the case, where the difference in the decay rates between the inphase and antiphase terms of the density matrix is much smaller than the coupling constant J, and the relaxation delay is much greater than $1/J$, the relaxation rates of $I^{\pm}$ may be approximated as $\lambda \pm \eta$, where λ is the average of the inphase and antiphase decay rates and η is the cross-correlation rate due to interference effects between the CSA of spin I and the IS dipolar coupling. In the case of an axially symmetric chemical shift tensor with principal axis coincident with the dipolar interaction vector, η can be expressed as

$$\eta = -\frac{1}{6}\frac{\mu_0}{4\pi}\frac{\gamma_I^2\gamma_S\eta}{r_{IS}^3}\Delta\sigma B_0[4J^x(0) + 3J^x(\omega_I)], \qquad [1]$$

where r_{IS} is the IS internuclear distance; $\Delta\sigma = \sigma_{\parallel} - \sigma_{\perp}$, is the difference of $\sigma_{\parallel}$ and $\sigma_{\perp}$, the parallel and perpendicular components of the principal chemical shift tensor; and $J^x(0)$ and $J^x(\omega_I)$ are values of the cross-correlation spectral density functions The cross-correlation spectral density functions $J^x(\omega)$ are defined by

$$J^x(\omega) = \int_0^{\infty} G^{cd}(t)\cos(\omega t)dt, \qquad [2]$$

where $G^{cd}(t)$ is the cross-correlation function for chemical shift anisotropy–dipolar coupling interference effects (see Appendix). The latter are in general different from the autocorrelation spectral density functions, $J^a(\omega)$.

The situation becomes rather complicated if the overall tumbling of the molecule is anisotropic (*16*), but some simplification occurs when the rotational diffusion is axially symmetric. The cross-correlation spectral density functions, in this case, are given by (see Appendix) (*2*)

$$J^x(\omega) = \sum_{l=0}^{2}\frac{(S_x^l)^2\tau_l}{1+\omega^2\tau_l^2} + \frac{[A_l^x - (S_x^l)^2]\tau}{1+\omega^2\tau^2}, \qquad [3]$$

where $\tau_0 = (6D_2)^{-1}$, $\tau_1 = (D_1 + 5D_2)^{-1}$, $\tau_2 = (4D_1 + 2D_2)^{-1}$, and $1/\tau = 1/\tau_e + 2\,\mathrm{Tr}[D] = 1/\tau_e + (2D_1 + 4D_2)$ (it has been assumed that $\tau_e \ll 1/D_1, 1/D_2$). Here, D is the diffusion tensor; D_1 and D_2 are the principal elements of the diffusion tensor which are parallel and perpendicular to its unique axis (*2*). S_x^l is a component of the generalized order parameter, S_x (defined in the Appendix), for CSA–dipole cross-correlation, and $\tau_e = (6D_{eff})^{-1}$ is the correlation time for internal motion which occurs on a timescale which is much faster than the overall tumbling (D_{eff} is the effective diffusion constant for the internal motion (*17*). The coefficients A_l^x are given by

$$A_0^x = \tfrac{1}{4}(3\cos^2\theta_c - 1)(3\cos^2\theta_d - 1)$$

$$A_1^x = \tfrac{3}{4}\sin(2\theta_c)\sin(2\theta_d)\cos[\phi_c - \phi_d]$$

$$A_2^x = \tfrac{3}{4}\sin^2(\theta_c)\sin^2(\theta_d)\cos[2(\phi_c - \phi_d)], \qquad [4]$$

where θ_c and θ_d are the angles made by the unique axis of the shift tensor and the internuclear vector, with the unique axis of the diffusion tensor, respectively, and ϕ_c and ϕ_d are the corresponding azimuthal angles (*2*, *18*). As shown in the Appendix, in the absence of internal motion, $(S_x^l)^2 = A_l^x$.

The autocorrelation spectral density functions are given by (see Appendix)

$$J^a(\omega) = \sum_{1=0}^{2}\frac{(S_a^l)^2\tau_l}{1+\omega^2\tau_l^2} + \frac{[A_l^a - (S_a^l)^2\tau]}{1+\omega^2\tau^2}. \qquad [5]$$

As in the case of cross correlation, in the absence of internal motion, $(S_a^l)^2 = A_l^a$. The coefficients, A_l^a, for the autocorrelation spectral density functions are given by

$$A_0^a = \tfrac{1}{4}(3\cos^2\theta_d - 1)^2$$

$$A_1^a = \tfrac{3}{4}\sin^2(2\theta_d)$$

$$A_2^a = \tfrac{3}{4}\sin^4(\theta_d). \qquad [6]$$

In order to obtain expressions analogous to conventional Lipari–Szabo theory (*17*), we express the auto- and cross-correlation spectral density functions using effective order parameters, as

$$J^x(\omega) = S_x^2\sum_{l=0}^{2}\frac{A_l^x\tau_l}{1+\omega^2\tau_l^2} + \frac{(1-S_x^2)\tau}{1+\omega^2\tau^2} \qquad [7]$$

$$J^a(\omega) = S_a^2\sum_{l=0}^{2}\frac{A_l^a\tau_l}{1+\omega^2\tau_l^2} + \frac{(1-S_a^2)\tau}{1+\omega^2\tau^2}. \qquad [8]$$

However, it should be realized that, in general, defining one order parameter for the internal motion is not possible when the overall motion is not isotropic (see Appendix). We see that the "order parameters" for cross correlation in [7] and for autocorrelation in [8] both give an indication of local order, or a lack of it, but there is no simple relationship between the two, and thus, they would not correlate very well, even in the absence of anisotropic local motion.

Things are simplified greatly for isotropically tumbling mol-

ecules. In this case, the cross-correlation functions are given by (see Appendix)

$$J^{x}(\omega) = \frac{S_x^2\tau_c}{1 + \omega^2\tau_c} + \frac{(P_2[\cos(\theta_{cd})] - S_x^2)\tau}{1 + \omega^2\tau^2}, \qquad [9]$$

where $\tau_c = (6D)^{-1}$ is the rotational correlation time, $1/\tau = 1/\tau_c + 1/\tau_e$, and θ_{cd} is the angle between the principle axis of the shift tensor and the internuclear vector. This is identical to the expression obtained by Fischer *et al.* (*19*). In this case, complete separation of the overall and internal motion is possible and the internal motion can be represented by a single order parameter. The corresponding autocorrelation function is given by (see Appendix)

$$J^{a}(\omega) = \frac{S_a^2\tau_c}{1 + \omega^2\tau_c^2} + \frac{(1 - S_a^2)\tau}{1 + \omega^2\tau^2}. \qquad [10]$$

For most reasonable models of motion of nuclei in the peptide plane, the cross-correlation order parameter may be approximated by $S_x^2 = P_2[\cos(\theta_{cd})]S_a^2$, when θ_{cd} is small. Using this in [9] and comparing with [10], we have

$$J^{x}(\omega) = P_2[\cos(\theta_{cd})]J^{a}(\omega). \qquad [11]$$

Using [11] in [1], we have for an isotropically tumbling molecule with an axially symmetric chemical shift tensor

$$\eta = -\frac{1}{6}\frac{\mu_0}{4\pi}\frac{\gamma_I^2\gamma_S\eta}{r_{IS}^3}\Delta\sigma\frac{1}{2}(3\cos^2\theta_{cd} - 1)B_0[4J^{a}(0) + 3J^{a}(\omega_I)], \qquad [12]$$

It is possible to extend [1] to the case where the chemical shift tensor is not axially symmetric. In that case it may be written as a sum of two axially symmetric shift tensors each with its unique axis (*1*) allowing [1] to be rewritten as

$$\eta = -\frac{1}{6}\frac{\mu_0}{4\pi}\frac{\gamma_I^2\gamma_S\eta}{r_{IS}^3}B_0\sum_{k=1,2}\Delta\sigma_k[4J^{x(k)}(0) + 3J^{x(k)}(\omega_I)], \qquad [13]$$

where $\Delta\sigma_1 = \frac{1}{2}(\sigma_{33} - \sigma_{11})$ and $\Delta\sigma_2 = \frac{1}{2}(\sigma_{33} - \sigma_{22})$ are the effective anisotropies for the two axially symmetric parts of the shift tensor and σ_{ii} $(i = 1, 2, 3)$ are the principal components of the shift tensor. In the case of a spherically symmetric molecule, which tumbles isotropically, this, in analogy to [12], yields

$$\eta = -\frac{1}{6}\frac{\mu_0}{4\pi}\frac{\gamma_I^2\gamma_S\eta}{r_{IS}^3}[\Delta\sigma_1 P_2(\cos(\theta_{cd}^1)) + \Delta\sigma_2 P_2(\cos(\theta_{cd}^2))] \times [4J^{a}(0) + 3J^{a}(\omega_I)], \qquad [14]$$

where θ_{cd}^1 and θ_{cd}^2 are the angles made by the two axially symmetric components of the shift tensor with the IS internuclear vector. The quantity within the brackets in [14] is the projection of the anisotropy of the shift tensor on the IS internuclear vector and is represented by $\Delta\sigma'$. However, it should be remembered that [14] is a crude approximation since both θ^1 and θ^2 cannot be close to zero at the same time.

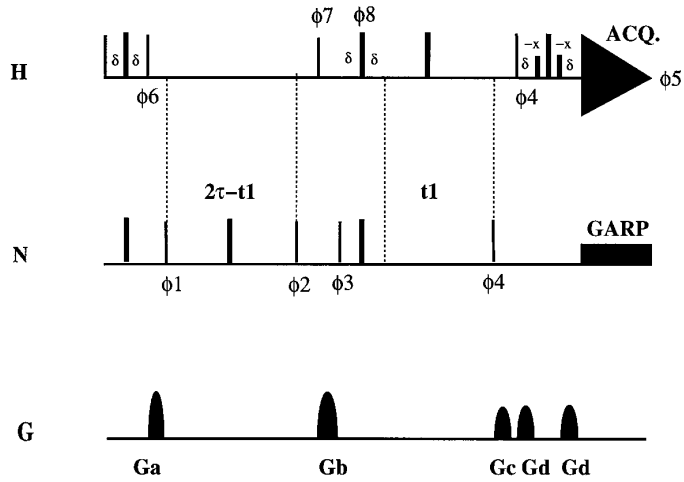

FIG. 1. Experiments to estimate η_N. Scheme I: The narrow and thick lines represent $\pi/2$ and π pulses, respectively. The short thick bars at the end of the experiment represent selective $\pi/2$ pulses on water. All pulses are along the x-axis unless otherwise stated. $\phi_1 = \{x, -x\}$; $\phi_2 = \{2(x), 2(-x)\}$; $\phi_3 = \{x\}$; $\phi_4 = \{4(x), 4(-x)\}$; $\phi_5 = \{2(x), 2(-x)\}$; and $\phi_6 = \{y, -y\}$. Quadrature detection in t_1 is achieved by cycling ϕ_3 in a States–TPPI fashion. All gradients are 1.5 ms long and are of strength 29 G/cm, except G_a, which is 23.2 G/cm. The delay δ is set approximately 2.6 ms. G_a and G_d were along the x- and z-axes; G_b and G_c were along x- and y-axes. In scheme II, the ^{1}H $\pi/2$ pulse labeled ϕ_7, the ^{1}H π pulse labeled ϕ_8, and the gradient G_b were not applied.

EXPERIMENTAL DESIGN

The pulse sequences we propose for the measurement of the cross-correlation rate η_N are shown in Figs. 1a and 1b. An inspection of these sequences reveals that they are, in essence, identical to those proposed by Tjandra *et al.* (*2*), except for one major difference—the relaxation delay is decremented with the evolution time, in an accordion (*20–23*) fashion. Thus, it has a value of 2τ for the very first t_1 point and a value of $2\tau - t_1$ at an intermediate t_1 point. Both schemes are based on the following principle: one starts with a density operator given by $2I_yS_z$ at the beginning of the relaxation delay, and the two components of the antiphase doublet, represented by $\frac{1}{2}(2I_yS_z \pm I_y)$, relax with relaxation rates given by $\lambda \pm \eta$. This differential relaxation causes a buildup of the in-phase component I_y at the end of the relaxation period, $2\tau - t_1$. For the very first t_1 point, the relevant portion of the density matrix after the relaxation delay (which in this case is equal to 2τ) may be expressed as $2I_yS_z[e^{-2(\lambda+\eta)\tau} + e^{-2(\lambda-\eta)\tau}] + I_y[e^{-2(\lambda+\eta)\tau} - e^{-2(\lambda-\eta)\tau}]$. For

any arbitrary t_1 point, the density matrix at the end of the relaxation period $(2\tau - t_1)$ may be represented by

$$\sigma(2\tau - t_1) = 2I_yS_z[e^{-(\lambda+\eta)(2\tau-t_1)} + e^{-(\lambda-\eta)(2\tau-t_1)}] + I_y[e^{-(\lambda+\eta)(2\tau-t_1)} - e^{-(\lambda-\eta)(2\tau-t_1)}]. \quad [15]$$

The scheme shown in Fig. 1 is designed to detect the component of the density matrix which is represented by I_y at the end of the relaxation period $(2\tau - t_1)$; we call this scheme I. The experiment to detect the $2I_yS_z$ component (called scheme II) is similar to that in scheme I, except that the ^{1}H $\pi/2$ pulse ϕ_7, ^{1}H π pulse ϕ_8, and gradient G_b are not applied. Assuming for the time being that chemical shift evolution can be made identical for the two schemes and these effects can be represented by a function $F(\omega, t_1)$, we obtain the signals in scheme I (Q_1) and scheme II (Q_2) at the beginning of the detection period as

$$\begin{aligned} Q_1 &= \langle I_y\rangle(2\tau) = K[e^{-2(\lambda+\eta)\tau}e^{+\eta t_1} - e^{-2(\lambda-\eta)\tau}e^{-\eta t_1}]F(\omega, t_1) \\ Q_2 &= \langle 2I_yS_z\rangle(2\tau) \\ &= K[e^{-2(\lambda+\eta)\tau}e^{+\eta t_1} + e^{-2(\lambda-\eta)\tau}e^{-\eta t_1}]F(\omega, t_1), \end{aligned} \quad [16]$$

where K is a constant which relates to the measured signal intensity. As is evident from Fig. 1, the length in time of the two schemes is the same and so are the relaxation losses (to a very good approximation); thus K is taken to be the same in both expressions (i.e., for Q_1 and Q_2). We construct two new datasets Q_σ and Q_δ, which are obtained by taking the sum and difference of the two signals. These are given by

$$\begin{aligned} Q_\sigma &= Q_2 + Q_1 = 2K[e^{-2(\lambda+\eta)\tau}]e^{+\eta t_1}F(\omega, t_1) \\ Q_\delta &= Q_2 - Q_1 = 2K[e^{-2(\lambda-\eta)\tau}]e^{-\eta t_1}F(\omega, t_1). \end{aligned} \quad [17]$$

The ratio of Q_δ to Q_σ gives a particularly simple dependence on the relaxation time τ. This is represented by

$$\frac{Q_\delta}{Q_\sigma} = e^{4\eta\tau}\left[\frac{e^{-\eta t_1}}{e^{+\eta t_1}}\right]. \quad [18]$$

The t_1 dependence can be removed by using the integrals of the Fourier-transformed t_1 datasets represented by the numerator and the denominator of [18]. Amplitudes of peaks in the transformed spectra can also be used if the value of η is small and identical window functions are used for the sum and difference datasets. Simulations with an η value of 4.0 s^{-1}, a 2τ value of 70 ms and a Kaiser window (argument 10) show that using peak amplitudes underestimates the value of η by ~15% (this decreases with decreasing η values), whereas using integrated intensities yields the correct value. We therefore chose the latter option.

In the above discussion we assumed that evolution of the relevant terms during t_1 was the same in the two schemes by using the same $F(\omega, t_1)$ for both Q_1 and Q_2 in [16]. This, however, is not the case. Consideration of the details of chemical shift evolution during t_1 shows that some additional data manipulation is required before taking the sum and differences as in [17]. Inspection of Fig. 1 reveals that after the relaxation period, $(2\tau - t_1)$, the magnetization is stored along z in both schemes. In scheme I, the ^{1}H $(\pi/2)_x$ pulse immediately after the relaxation period generates $-2I_zS_y$ magnetization (where I = ^{15}N and S = ^{1}H), and this is defocused using a gradient. The subsequent ^{15}N $(\pi/2)$ is cycled in a States–TPPI (*24*) fashion (x, y). In the case of scheme I, an ^{15}N $(\pi/2)_x$ creates $-I_y$ which at the start of the t_1 evolution period is $-2I_xS_z$. The evolution of this term during t_1 is given by $-2I_xS_z\cos(\omega t_1) - 2I_yS_z\sin(\omega t_1)$. Only the second term is finally detected since the first is converted to undetectable double quantum coherence. This point constitutes the real part of the complex magnetization, in t_1. The imaginary part is generated by the ^{15}N $(\pi/2)_y$ pulse, which creates I_x. At the beginning of t_1 this generates $2I_yS_z$, which evolves as $2I_yS_z\cos(\omega t_1) - 2I_xS_z\sin(\omega t_1)$. Again, only the $2I_yS_z$ part is detectable. Thus, the oscillatory part of the magnetization in scheme I may be represented as {Re part, Im part} = $\{-\sin(\omega t_1), \cos(\omega t_1)\}$. In scheme II, the ^{1}H $(\pi/2)_x$ pulse after the relaxation delay $(2\tau - t_1)$ and the gradient following it are not applied. Using similar arguments and a simple product operator treatment, as in the case of scheme I, we have, for scheme II, $\{\cos(\omega t_1), \sin(\omega t_1)\}$. To generate an identical evolution behavior to scheme I we first exchange real and imaginary parts for the signal in scheme II to get $\{\sin(\omega t_1), \cos(\omega t_1)\}$; then we replace ω by $-\omega$ (equivalent to complex conjugation) in the transformed signal for scheme II, to obtain $\{-\sin(\omega t_1), \cos(\omega t_1)\}$, which is identical to scheme I. This allows us to perform the addition and subtraction to generate the two datasets in [17].

The extension of the two schemes shown in Fig. 1 to an experiment to measure η for the cross correlation between ^{13}C′ CSA and ^{13}C′–^{15}N dipolar coupling is quite straightforward. The pulse sequences are based on an HNCO (*25*) type experiment as shown in Fig. 2 (scheme I). In the corresponding scheme II, the ^{15}N $\pi/2$ pulse ϕ_8 and the ^{15}N π pulse ϕ_9 are not applied. There are, however, a few important points to note. The two selective $^{13}C_\alpha$ pulses are applied during the relaxation period in order to prevent the buildup of terms like $2I_yM_z$ (I = ^{13}C′, M = $^{13}C_\alpha$) from $2I_yS_z$ (S = ^{15}N) due to cross correlation between the ^{13}C′–$^{13}C_\alpha$ and ^{15}N–^{13}C′ dipolar interactions (*26*) or the buildup of $4I_yM_zS_z$ due to cross correlation between the ^{13}C′ CSA and the ^{13}C′–$^{13}C_\alpha$ dipolar interaction. A gradient is also applied during the z-storage period after the relaxation delay in scheme II, which destroys some additional spurious terms.

The advantages of the above schemes in comparison to that originally proposed by Tjandra *et al.* (*2*) are open to debate. In fact, by taking appropriate sums, differences, and ratios of the two data sets collected by Tjandra *et al.*, an identical functional relationship between η and τ can be derived. However, the data collection in our case, for a given τ, is actually collected over a range of relaxation delays as t_1 is incremented. There may be

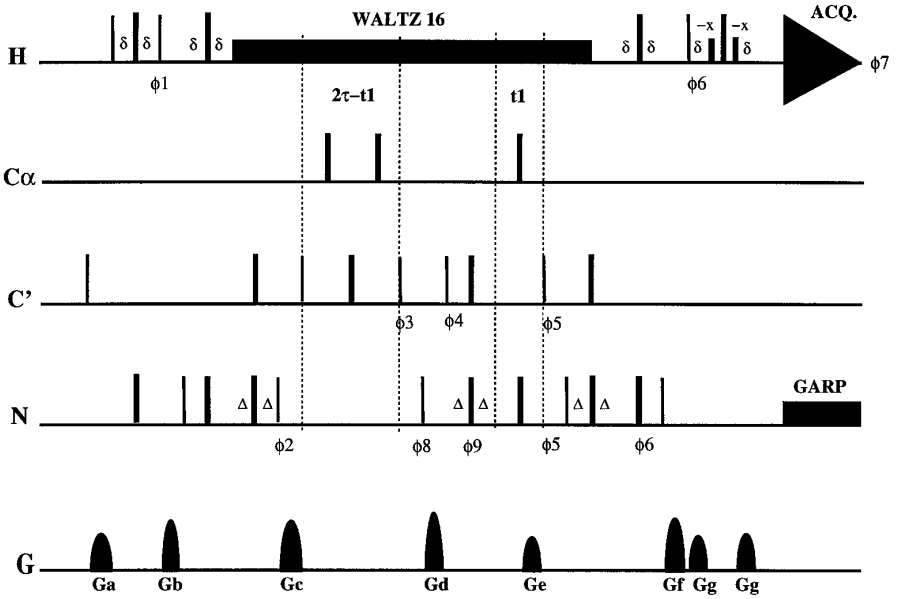

FIG. 2. Experiments to estimate η_C. Scheme I: The phase cycling is as follows: $\phi_1 = \{y, -y\}$; $\phi_2 = \{2(x), 2(-x)\}$; $\phi_3 = \{4(x), 4(-x)\}$; $\phi_4 = \{x\}$; $\phi_5 = \{8(x), 8(-x)\}$; $\phi_6 = \{16(x), 16(-x)\}$; and $\phi_7 = \{-x, 2(x), -x, x, 2(-x), x\}$. The $^{13}C_\alpha$ pulses are off-resonance square pulses. The $^{13}C'$ $\pi/2$ and π are adjusted in RF strength to be $\sqrt{15/(4\tau)}$ and $\sqrt{3/(2\tau)}$ in length, respectively, in order to prevent excitation of $^{13}C_\alpha$ (the carrier was placed in the center of the $^{13}C'$ region and τ is the difference in Hz between the center of the $^{13}C'$ region and the $^{13}C_\alpha$ region). The gradients G_a, G_b, G_c, and G_e are of duration 1.0 ms and have strengths 10.0, 20.0, −30.0, and 20.0 G/cm, respectively. G_d was of duration 1.5 ms and had a strength of 32.0 G/cm. The corresponding values of duration and strength for G_f and G_g were 2.0 ms and 32.0 G/cm, and 0.5 ms and 10.0 G/cm, respectively. The delays δ and Δ are approximately 2.6 and 12.5 ms, respectively. In scheme II, the ^{15}N $\pi/2$ pulse labeled ϕ_8 and the ^{15}N π pulse labeled ϕ_9 were not applied.

advantages in collecting over a range of relaxation times in that systematic errors that are τ dependent may average to a smaller value. There is also some advantage in having data presented in a form in which the option of directly extracting relaxation rates by fitting the t_1 time dependence presents itself (see Eq. [18]). In that case, where auto- and cross-relaxation rates are equal, the dependence of Q_δ is particularly simple. The autorelaxation rate, λ, in the case of ^{15}N, is dominated by the ^{15}N–^1H dipolar interaction at low field and is initially independent of the strength of the applied static magnetic field. The cross-correlation rate η, on the other hand, increases linearly with the applied static field strength. At appropriate high fields these two rates become equal. Peruvshin *et al.* have taken advantage of the cancelation of these two rates to maximize resolution in heteronuclear 2D experiments. It can be seen from [17] that under these conditions, and prior to Fourier transformation in t_1, the individual indirect FID, Q_δ, can be fit as a function of t_1 to obtain a value for η.

EXPERIMENTAL

The experiments to determine η_N were performed on a 3.0 mM ^{15}N-labeled sample of *E. coli* DnaJ(1–78) in phosphate buffer at pH 6.0, at 30°C. The preparation of the protein and its structural characterization have been discussed in previous publications (*28, 29*). Duplicate datasets for each scheme were collected using $2\tau = 75.0$ ms with 110 complex points in the ^{15}N dimension, acquiring 64 transients per indirect point. The number of points in the direct dimension was 512. The sweep widths in the direct and indirect dimensions were 6006.0 and 1519.0 Hz, respectively. The data in both dimensions were apodized using a Kaiser window and zero-filled to double the size (or to the nearest power of 2) prior to Fourier transformation. A series of spectra were also collected with $2\tau = 52.0$, 62.0, 72.0, 82.0, 92.0, and 102.0 ms, with matrix sizes of $64(t_1) \times 512(t_2)$, with 32 transients collected per t_1 point. The indirect sweep width in these cases was taken to be 1538.0 Hz. The data were processed in the same way as above. The delay between scans was set to 2.0 s for all the above experiments. All experiments to determine η_N were performed on GE Omega spectrometer operating at a ^1H frequency of 500 MHz and equipped with a triple resonance probe capable of generating magnetic field gradients along all three axes.

The experiments to determine η_C were performed on a 2.0 mM ^{15}N, ^{13}C-labeled sample of *E. coli* DnaJ(1–78) in phosphate buffer at pH 6.0, at 30°C. Duplicate sets of data were collected for each scheme with $2\tau = 50.0$ 65.0 ms. One hundred twenty complex t_1 points were collected with a sweep width of 2500.0 Hz in the $^{13}C'$ dimension, with 64 transients per t_1 point; 256 complex points were collected in the direct dimension with a sweep width of 6000.0 Hz. The recycling delay was set to 2.0 s as in the case of the ^{15}N experiments. A $\pi/2$ pulse on $^{13}C'$, followed by the application of a gradient, at the start of the experiment, helped destroy the $^{13}C'$ magnetization. The data were processed in the same way as in the case

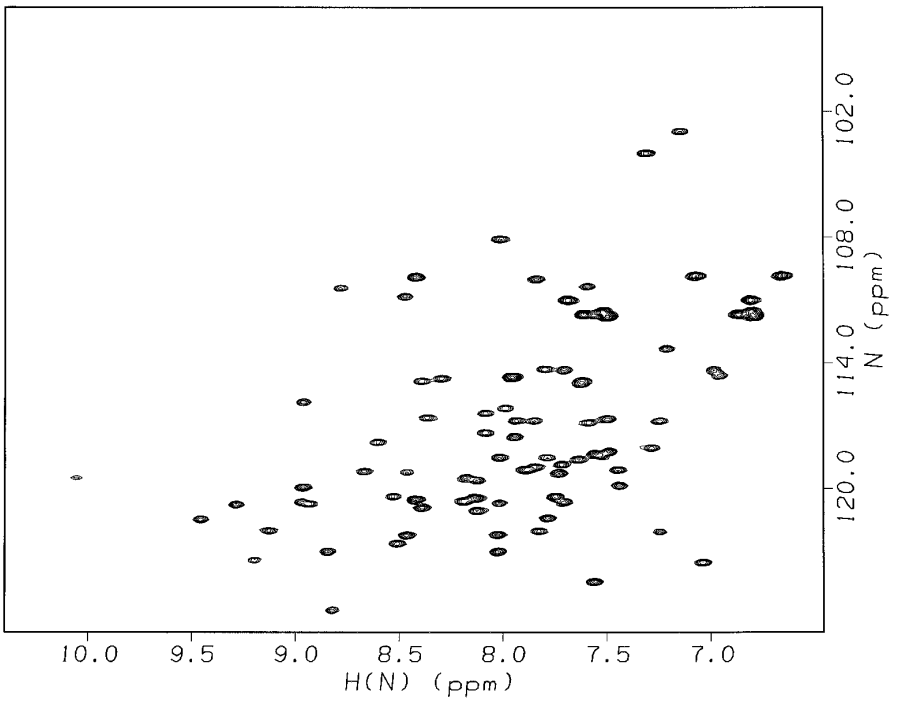

FIG. 3. The sum dataset from the experiment to determine η_N in ^{15}N-labeled *E. coli* DnaJ(1–78). The difference dataset is similar in appearance.

of the η_N data. All the ^{13}C data were collected on a Varian Unity spectrometer operating at a ^{1}H frequency of 500 MHz, equipped with a triple-resonance probe capable of generating magnetic field gradients along the *z*-axis. All data were processed using the Felix 95.0 suite of programs available from Biosym/MSI, San Diego, CA.

RESULTS AND DISCUSSION

The sum dataset for the ^{15}N case is shown in Fig. 3 (the difference dataset is visually similar). This resembles an HSQC spectrum. The spectrum shows very good dispersion in both ^{15}N and ^{1}H dimensions, and the values of η_N can be measured for 62 (well-resolved) out of the 78 residues. The signal buildup as a function of the delay, 2τ, for a few residues is shown in Fig. 4. η_N estimated from the buildup curves using a nonlinear least squares fit to [18] yielded values which were consistent with those obtained directly from [18] for a given value of 2τ. The fits to [18] were performed using the ODRPACK subroutines (*30*).

Individual t_1 FIDs for the sum (Q_σ) and difference (Q_δ) were also analyzed for a few select residues for the 75-ms dataset (results not shown). The FIDs were obtained by selecting a crosspeak in transformed Q_σ and Q_δ spectra loading a column through a given ^{15}N chemical shift and then inverse Fourier transforming in the t_1 dimension. The values of η were estimated from the FIDs by Bayesian analysis using the program XRambo (*31*). In this case some effort must be made to take account of leakage from nearby columns. On inverse Fourier transformation, the FID obtained may contain components due to those resonances with ^{15}N chemical shifts close to the one in question. In the Bayesian analysis, the frequencies of these resonances were supplied along with the frequency of the resonance in question, and the corresponding η values were extracted. The values of η thus obtained were consistent with those obtained directly from [18] though the errors were 5–6% larger for the residues considered.

The η_N values displayed in Fig. 5 were estimated from the 75.0-ms datasets using [18] directly. This method was the least time consuming and as mentioned above produced results consistent with the other two methods, i.e., nonlinear least squares fits for various τ values and Bayesian estimation of η values from the Q_σ and Q_δ interferrograms. The random errors were estimated from two identical experiments. The values of η_N seem to be quite uniform over the DnaJ(1–78) sequence having an average of $4.0 \pm 0.8\ s^{-1}$. The average values are consistent with those expected for a protein this size (*4a, 32*). Some smaller values were found at the N and C terminal ends and near residues 34, 38, 41, 53, and 64. Residues 34, 38, and 41 are part of an extended loop between α helices which end at residue 31 and begin at residue 41 and lower values may be reflecting shorter correlation times (*28*). Increased mobility for this region is also reflected in ^{15}N relaxation rates and NOEs.

The origin of the decrease at 53 and 64 is less clear. The ^{15}N chemical shift tensor is known to be almost axially symmetric with the principal axis of the shift tensor making an angle of 20–24° with respect to the NH internuclear vector. The magnitude of $\Delta\sigma$ is about -160 ppm (*33–35*). Variation in these values could lead to the noted decreases, but existing data suggest that these values seldom vary over the protein backbone (*2*).

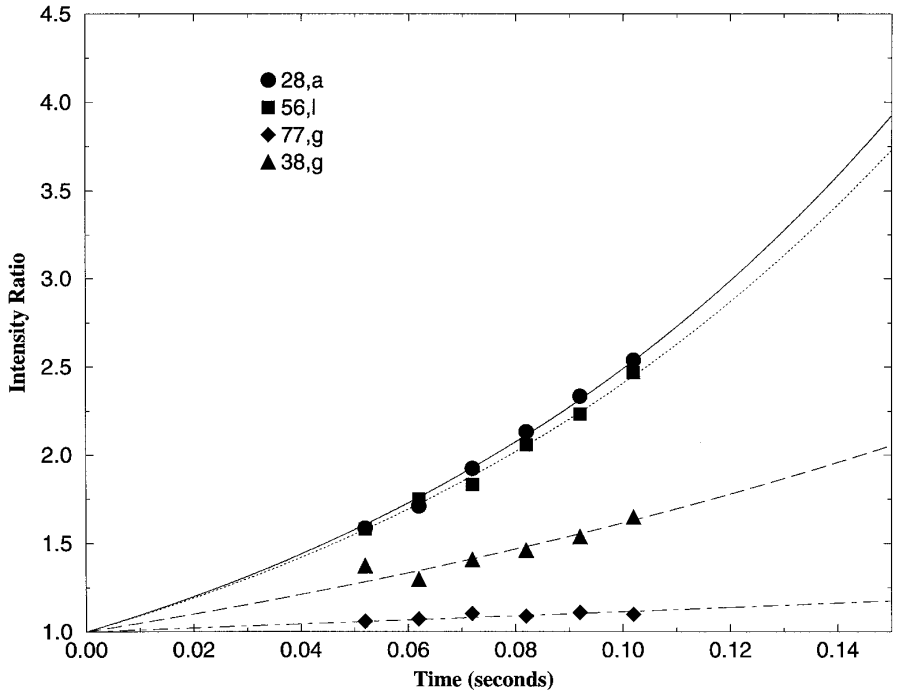

FIG. 4. Buildup of the signal (for the experiments to determine η_N) as a function of relaxation delay 2τ, plotted for selected residues, showing the range of buildup rates (η_N).

It is to be mentioned here that DnaJ(1–78) is a highly nonspherical protein; the principal moments of inertia are in the ratio 1.0:0.91:0.26 (almost axially symmetric). Thus the overall tumbling of DnaJ(1–78) can be considered highly anisotropic though axially symmetric. For a protein this anisotropic, it is to be expected that there would be some variation in relaxation behavior due to different angles of interaction vectors with respect to diffusion axes. There would also be

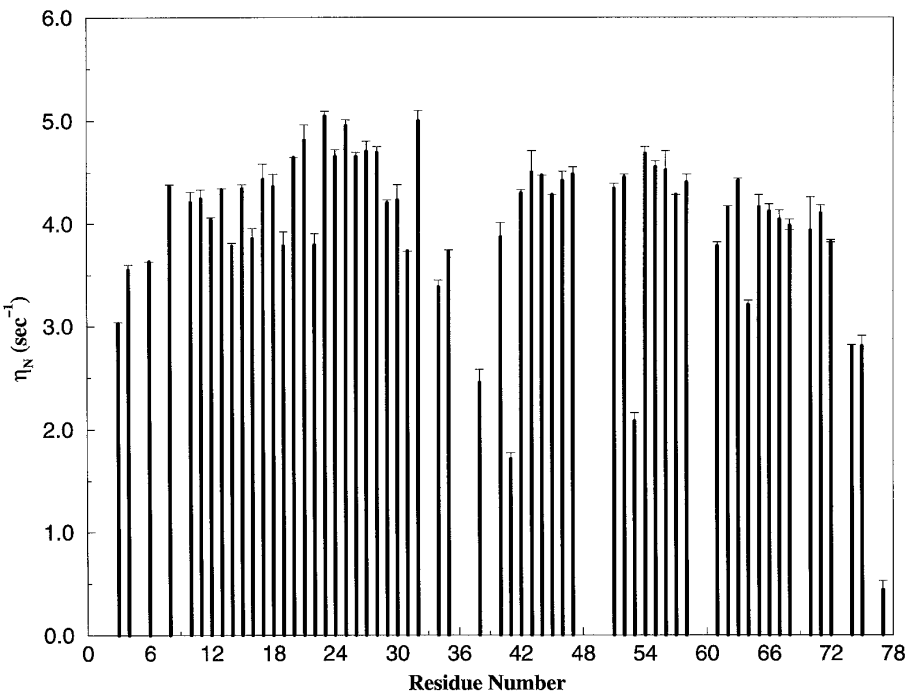

FIG. 5. Values of η_N plotted against residue number for *E. coli* DnaJ(1–78).

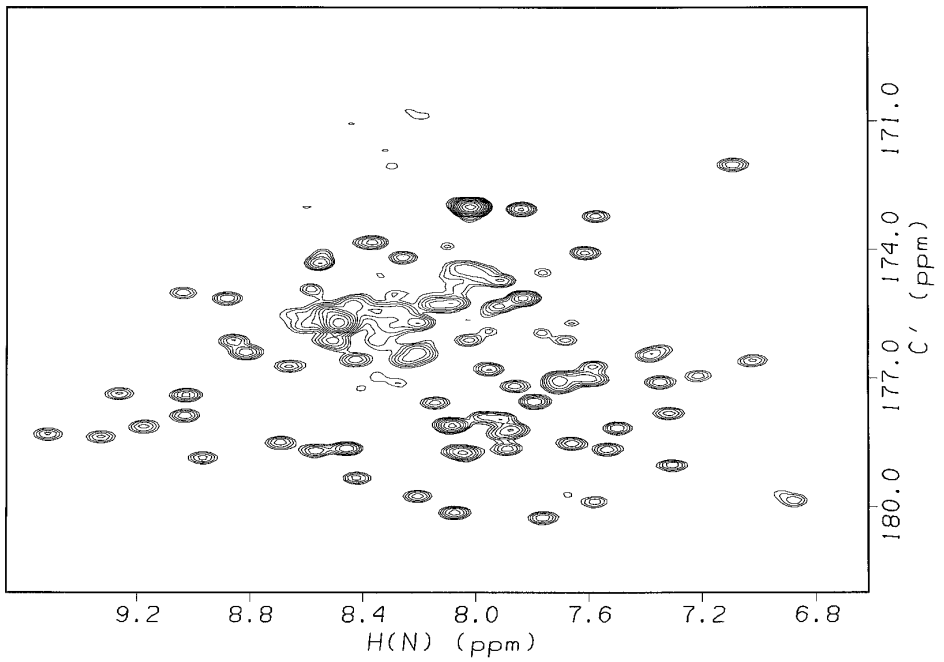

FIG. 6. The sum dataset from the experiment to determine η_C in ^{15}N,^{13}C-labeled *E. coli* DnaJ(1–78). The difference dataset is similar in appearance.

some divergence of the cross-correlation- and autocorrelation-dependent relaxation parameters. However, these vanish as the angle between the principal axis of the ^{15}N shift tensor and the NH internuclear vector becomes small. Thus, some of the variation in Fig. 5 may also come from the anisotropic overall tumbling of the protein.

A spectrum resulting from the sum dataset for the ^{13}C experiments is shown in Fig. 6 (the difference dataset is visually similar). This resembles a 2D HNCO (*25*) spectrum with the indirect dimension yielding $^{13}C'$ chemical shifts and the direct dimension yielding amide ^1H chemical shifts. The dispersion is moderately good in the indirect dimension and can be improved by extending the experiment to three dimensions by using amide ^{15}N evolution. As is shown in Fig. 7, the values of η_C show a larger deviation along the DnaJ(1–78) sequence than in the case of the η_N values. The average value for 51 (well-resolved) of the 78 residues was -0.9 ± 0.4 s^{-1}, a reasonable number in view of expectations for a molecule of this size. But, the variation is at first surprising.

As in the case of ^{15}N, both differences in $\Delta\sigma$ and $J(\omega)$ could contribute to the variation in the values of η_C over the protein backbone. But, unlike the ^{15}N case, there is reason to expect some variation in $\Delta\sigma$ due to hydrogen bonding and other effects. Ideally we would like to separate $\Delta\sigma$ and $J(\omega)$ effects so these variations can be observed. If we assume a model where the same $J(\omega)$ terms contribute to both η_N and η_C, as would be the case in an isotropic model, we can attempt to separate contributions due to variations in $J(\omega)$ and $\Delta\sigma$. This, of course, is not strictly valid for DnaJ(1–78) but can, nevertheless, be instructive. Under this assumption, η_N rates can be used to estimate $J^a(0)$ from [12]. It can be further assumed that since the NH and the NC vectors are part of an approximately rigid peptide unit, they experience similar local motion and hence share the same autocorrelation spectral density function $J^a(0)$. It would then be possible to obtain a measure for $\Delta\sigma'$ which is the projection of the $^{13}C'$ CSA on the NC internuclear vector by using the expression

$$\Delta\sigma' = \frac{\eta_C}{\eta_N}\left(\frac{\gamma_N\gamma_H}{\gamma_C^2}\right)\left(\frac{r_{NC}}{r_{NH}}\right)^3 \frac{(3\cos^2\theta - 1)}{2}\Delta\sigma_N. \quad [19]$$

Here $\Delta\sigma_N$ is the chemical shift anisotropy of ^{15}N (assumed to be -170.0 ppm), θ is the angle between the NH internuclear vector and the principal axis of the ^{15}N chemical shift tensor (assumed to be 20°), r_{NH} is the N–H bond length (taken to be 1.02 Å) and the r_{NC} is the N–C bond length (taken to be 1.32 Å). The apparent values of $\Delta\sigma'_C$ thus obtained are plotted in Fig. 8 against residue number. We obtain an average value of -77 ± 36 ppm, over the protein backbone. It is encouraging to note that, despite the crudeness of the assumptions, the average value obtained is consistent with that calculated using principal values of the shift tensor measured in the solid state (*34*). Assuming experimental values of σ_{11}, σ_{22}, and σ_{33} for Z-acetanilide from (*34*) and $\theta_1 = 30°$, $\theta_2 = 120°$, and $\theta_3 = 90°$, we obtain a value of -88 ppm for $\Delta\sigma'_C$.

The absolute values of $\Delta\sigma'_C$ obtained in the helical regions of the protein seemed in general to be lower than those found in the nonhelical regions. Considering those residue types found in both helical and nonhelical regions of the protein, we see that this is indeed true. There are three glutamine residues in nonhelical regions; these show an average value of -91 ± 12

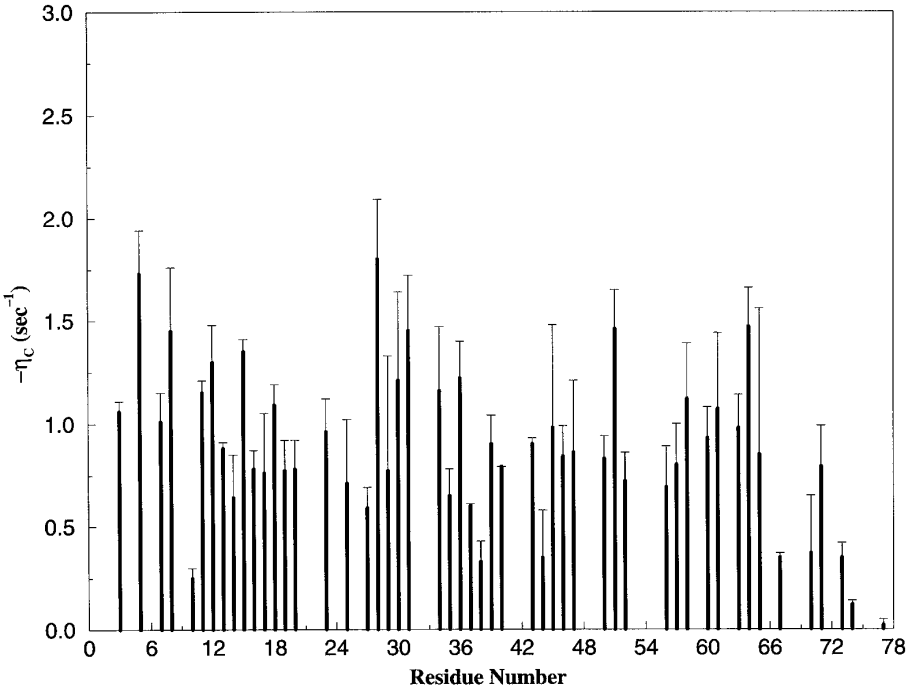

FIG. 7. Values of η_C plotted against residue number for *E. coli* DnaJ(1–78).

ppm for $\Delta\sigma'_C$ as opposed to a value of -30 ± 2 ppm for the lone glutamine residue found in the helical region. For lysine residues (two residues) and an alanine residue (one residue), the values in the nonhelical regions are -120 ± 40 and -121 ± 6 ppm, respectively. While the corresponding values in the helical regions for these two residue types (five lysines and seven alanines) are -79 ± 10 and -95 ± 20 ppm, respectively. It has been suggested that helical regions tend to be more strongly hydrogen-bonded than the corresponding nonhelical regions (*10*). Estimating the principal values of the

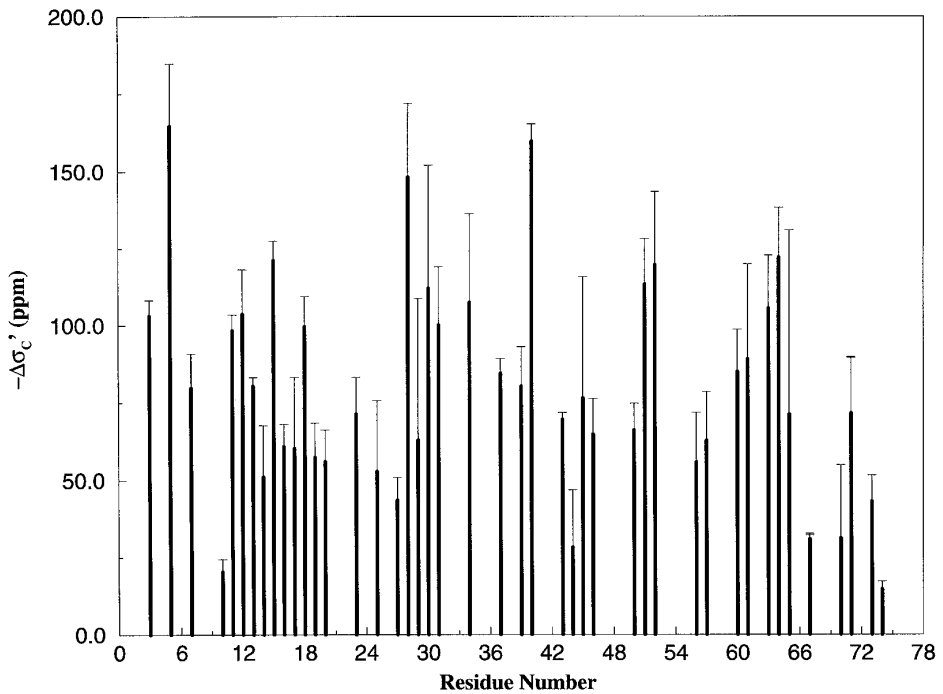

FIG. 8. Values of $\Delta\sigma'_C$ plotted against residue number for *E. coli* DnaJ(1–78).

$^{13}C'$ shift tensor from Fig. 2 of (*10*) for strongly and weakly hydrogen-bonded systems, and θ values as before, we find that $\Delta\sigma'_C$ should have a smaller absolute value in regions of strong hydrogen bonding than in those of weak hydrogen bonding by about 20 ppm. Two of the best defined helices in DnaJ(1–78) run from residues 16–31 and 41–56. Examination of Fig. 8 shows some suggestion of a trend toward lower absolute values in these regions with a few higher values in the loop at the end of the 16–31 helix.

Establishing a more concrete correlation would require application to a more symmetric protein and possibly some improvement in experimental precision. As illustrated in Eqs. [3]–[4] and [14], consideration of anisotropic diffusion and the nonaxially symmetric shift tensor introduces additional variables that complicate separation. There could also be several sources of error in the measured η values. Among these is the fact that we have used selective pulses on $^{13}C_\alpha$ in the experiments to determine η_C, in order to remove interference effects due to cross correlation between $^{13}C'$ CSA and $^{13}C'$–$^{13}C_\alpha$ dipolar couplings and that between the ^{15}N–$^{13}C'$ and $^{13}C'$–$^{13}C_\alpha$ dipolar couplings. This is only correct to first order (*36*). Incomplete inversion of the $^{13}C_\alpha$ would lead to further errors.

Despite the limitations presented above, we have presented here a set of experiments which demonstrate an ability to measure cross-correlation rates for both ^{15}N and $^{13}C'$ sites along a protein backbone. These rates normally depend on both dynamics and projection of CSA tensors on dipolar vectors. In the case of the ^{15}N cross-correlation rates, and spherical or nearly spherical proteins, it is possible to separate these effects because the ^{15}N shift tensor is axially symmetric and the angle made by the principal axis of the shift tensor with the NH internuclear vector is small, leading to a simple relationship between cross-correlation spectral density functions and autocorrelation spectral density functions. Autocorrelation spectral densities can be estimated from ^{15}N relaxation experiments and CSA values determined. However, the ^{15}N shift tensor proves not to be very sensitive to structural variations along the protein backbone. The case of $^{13}C'$ is more interesting, with preliminary results showing a qualitative correlation between CSA projections and hydrogen bonding. But, here, accurate separation of the structural and dynamic contributions to the cross-correlation rates is very difficult even in the case of spherical molecules. This is because the $^{13}C'$ shift tensor is not axially symmetric. One hopeful note is that it may be possible to study the effects of cross correlation of the $^{13}C'$ CSA with two different internuclear vectors such as ^{15}N–$^{13}C'$ (as done here) and $^{13}C'$–$^{13}C_\alpha$. These two vectors make a fixed angle with respect to each other and are part of the same amide bond, allowing one to assume that they experience similar local motion. This may allow more insight into variations of the $^{13}C'$ CSA with structure in proteins.

APPENDIX

Exact expressions for cross-correlation functions involving chemical shift anisotropy and dipolar coupling interactions can be derived in the limit of an axially symmetric chemical shift tensor and when the overall tumbling is axially symmetric. The derivations are based on those due to Szabo (*37*). A more complete treatment can be found elsewhere (*38*). The relevant cross-correlation function, $G^{cd}(t)$, in this case can be written as

$$G^{cd}(t) = \frac{2}{5}\langle P_2[e_c(t)\cdot e_d(0)]\rangle, \qquad [1]$$

where $e_c(t)$ and $e_d(0)$ are the unit vectors in the directions of the principal axis of the shift tensor at time t and that along the IS internuclear vector at time 0, respectively. Using the spherical harmonic addition theorem (*39*), [1] can be rewritten as

$$G^{cd}(t) = \sum_{m=-2}^{2}\langle D^{2*}_{m0}(\Omega_c(t))D^2_{m0}(\Omega_d(0))\rangle, \qquad [2]$$

where $\Omega_c(t)$ and $\Omega_d(0)$ are the orientation of the principal axis of the shift tensor at time t and that of the IS internuclear vector at time 0 in the lab frame, respectively. In order to separate the internal and overall motion, we transform into the molecular frame (principal axis frame of the diffusion tensor) in which the z-axis lies along the direction of the principal component of the axially symmetric diffusion tensor. Thus, [2] transforms to

$$G^{cd}(t) = \frac{2}{5}\sum_{lmn}\langle D^{2*}_{ml}(\Omega_M(t))\,D^{2*}_{l0}(\Omega_{c'}(t)) \times D^2_{mn}(\Omega_M(0))\,D^2_{n0}(\Omega_{d'}(0))\rangle, \qquad [3]$$

where $\Omega_M(t)$ and $\Omega_M(0)$ denote the orientation of the principal axis of the diffusion tensor in the lab frame at time t and 0, respectively. $\Omega'_c(t)$ and $\Omega'_d(0)$ are the orientations of the principal axis of the shift tensor and the internuclear vector in the molecular frame, respectively. If the overall motion and the internal motion occur on timescales which are very different from each other, the averaging of the two parts in [3] may be performed separately, and we have

$$G^{cd}(t) = \frac{2}{5}\sum_{lmn}\langle D^{2*}_{ml}(\Omega_M(t))\,D^2_{mn}(\Omega_M(0))\rangle \times \langle D^{2*}_{l0}(\Omega_{c'}(t))\,D^2_{n0}(\Omega_{d'}(0))\rangle, \qquad [4]$$

where the first term in brackets in [4] signifies the overall tumbling of the molecule and the second term denotes the

internal motion. For an axially symmetric diffusive overall motion we have

$$\sum_m \langle D^{2*}_{ml}(\Omega_M(t))\, D^2_{mn}(\Omega_M(0))\rangle = \delta_{ln}\exp[-(6D_2 + l^2(D_1 - D_2))t], \quad [5]$$

where D_1 and D_2 are the principal values of the diffusion tensor parallel and perpendicular to the unique axis of the diffusion tensor, respectively, and δ_{ln} is the Kronecker delta symbol. Using [5] in [4] we have

$$G^{cd}(t) = \sum_{l=-2}^{2} \exp[-(6D_2 + l^2(D_1 - D_2))t] \times \langle D^{2*}_{l0}(\Omega_{c'}(t))\, D^2_{l0}(\Omega_{d'}(0))\rangle. \quad [6]$$

In the absence of internal motion Ω'_c and Ω'_d are time-independent and [6] transforms to

$$G^{cd}(t) = \frac{2}{5}\sum_{l=0}^{2} \exp[-6D_2 + l^2(D_1 - D_2))t] \times d^2_{l0}(\theta_c) d^2_{l0}(\theta_d)\cos[l(\phi_c - \phi_d)] = \frac{2}{5}\sum_{l=0}^{2} A^x_l \exp[-(6D_2 + l^2(D_1 - D_2))t], \quad [7]$$

where θ_c and θ_d are the angles made by the principal axis of the shift tensor and the internuclear vector with the unique axis of the diffusion tensor, respectively, and ϕ_c and ϕ_d are the corresponding azimuthal angles. For a spherically symmetric molecule, $D_1 = D_2 = D$ and [6] transforms to

$$G^{cd}(t) = \frac{2}{5}\exp[-6Dt]\sum_{l=-2}^{2} D^{2*}_{l0}(\Omega_{c'})\, D^2_{l0}(\Omega_{d'}) = \frac{2}{5}\exp[-6Dt]P_2[\cos(\theta_{cd})], \quad [8]$$

where θ_{cd} is the angle between the principal axis of the shift tensor and the IS internuclear vector.

In the presence of internal motion, it can be seen from [6] that one can separate overall and internal motion only for a given value of l, in the general case. It is known that the correlation function can be approximated by (exact at $t = 0$ and $t = \infty$)

$$G^{cd}(t) = G^{cd}(\infty) + [G^{cd}(0) - G^{cd}(\infty)]\exp[-6D_{eff}t], \quad [9]$$

where D_{eff} is an effective diffusion constant for the internal motion. From [6], we see that $G_{cd}(0)$ is given by [7]. There is no closed form expression for $G^{cd}(\infty)$, in the general case. However, it is correct to assume that the interactions between the CSA and IS dipolar interactions are scaled down due to local motion for each given value of l in [6]. In that case, $G^{cd}(\infty)$ can be approximated as

$$G^{cd}(\infty) = \frac{2}{5}\sum_{l=0}^{2} \exp[-(6D_2 + l^2(D_1 - D_2))t](S^l_x)^2, \quad [10]$$

where $(S^l_x)^2 = \langle d^2_{10}(\theta_c)\cos(l\phi_c)\rangle\langle d^2_{10}(\theta_d)\cos(l\phi_d)\rangle + \langle d^2_{10}(\theta_c)\sin(l\phi_c)\rangle\langle d^2_{10}(\theta_d)\sin(l\phi_d)\rangle$. It can be seen that the S^l_x transform has components of a symmetric, rank 2 tensor which we call S_x. These are generalized order parameters for the cross correlation between the chemical shift anisotropy and dipolar coupling interactions. It should be realized that in the absence of internal motion $(S^l_x)^2 = A^x_l$ and we have the equality

$$\sum_{l=0}^{2} S^l_x = \sum_{l=0}^{2} A^x_l = P_2[\cos(\theta_{cd})]. \quad [11]$$

Using [9] and [10], we have

$$G^{cd}(t) = \frac{2}{5}\sum_{l=0}^{2} \exp[-(6D_2 + l^2(D_1 - D_2))t] \times [(S^l_x)^2 + (A^x_l - (S^l_x)^2)\exp(-6D_{eff}t)]. \quad [12]$$

When the principal axis of the CSA and the IS internuclear vector are collinear, $\theta_c = \theta_d$ and $\phi_c - \phi_d = 0$ and we have $G^{cd}(t) = G^{cc}(t) = G^{dd}(t)$, and the cross-correlation function which is identical to the autocorrelation function is given by

$$G^{cc}(t) = \frac{2}{5}\sum_{l=0}^{2} \exp[-(6D_2 + l^2(D_1 - D_2))t] \times [(S^l_a)^2 + (A^a_l - (S^l_a)^2)\exp(-6D_{eff}t)], \quad [13]$$

where $(S^l_a)^2 = |\langle d^2_{10}(\theta_c)\rangle|^2 = |\langle d^2_{10}(\theta_d)\rangle|^2$. As above, in the absence of internal motion $(S^l_a)^2 = A^a_l$ and we have the equality

$$\sum_{l=0}^{2} S^l_a = \sum_{l=0}^{2} A^a_l = 1. \quad [14]$$

Thus, complete separation of internal and overall motion is not possible even in the case of autocorrelation functions, in the general case.

For a spherically symmetric molecule, $D_1 = D_2 = D$ and we have from [6],

$$G^{cd}(0) = \frac{2}{5}\exp[-6Dt]\sum_{l=-2}^{2}\langle D_{l0}^{2*}(\Omega_{c'})D_{l0}^{2}(\Omega_{d'})\rangle$$

$$= \frac{2}{5}\exp[-6Dt]P_2[\cos(\theta_{cd})]. \quad [15]$$

The cross-correlation function, $G^{cd}(\infty)$, is given by

$$G^{cd}(t) = \frac{2}{5}\exp[-6Dt]\sum_{l=-2}^{2}\langle D_{l0}^{2*}(\Omega_{c'})\rangle\langle D_{l0}^{2}(\Omega_{d'})\rangle$$

$$= \frac{2}{5}\exp[-6Dt]S_x^2, \quad [16]$$

where S_x is the generalized Lipari–Szabo order parameter for cross correlation. Using [13] and [14], we have

$$G^{cd}(t) = \frac{2}{5}\exp[-6Dt] \times [S_x^2 + (P_2(\cos(\theta_{cd})) - S_x^2)\exp[-6D_{eff}t]]. \quad [17]$$

Thus, complete separation of internal and overall motion is indeed possible for spherically symmetric molecules which undergo isotropic tumbling, and one can indeed represent the internal motion by a single order parameter which is a scalar and may be viewed as the trace of that in the axially symmetric case. For the autocorrelation function in this case, we have

$$G^{cc}(t) = \frac{2}{5}\exp[-6Dt][S_a^2 + (1 - S_a^2)\exp[-6D_{eff}t]], \quad [18]$$

where S_a is the commonly used Lipari–Szabo generalized order parameter. Comparing [15] and [16], we see that in the case of spherical molecules,

$$S_x^2 = S_a^2 P_2[\cos(\theta_{cd})]. \quad [19]$$

From [19] we see that S_x^2 can be positive or negative, less than or equal to S_a^2 depending on the value of θ_{cd}, i.e., the geometry of the system. It should be stressed here that [19] *does not* hold in the case of nonspherical molecules. Thus, one has to be very careful in comparing auto- and cross-correlation order parameters in nonspherical molecules; they are not expected to be related to each other in a simple way.

In the above discussion we assumed that the chemical shift tensor was axially symmetric. Generalization of the formalism to the case of nonaxially symmetric chemical shift tensors is straightforward, since any nonaxially symmetric rank 2 tensor can be written as a sum of two axially symmetric rank 2 tensors (*1*).

ACKNOWLEDGMENTS

We thank Dr. John Flanagan of the Brookhaven National Laboratory for making facilities available for the overexpression of *E. coli* DnaJ(1–78). We thank Jon Lapham of Yale University for useful discussions. This work was supported by Grant GM 33225 from the National Institutes of Health.

REFERENCES

1. M. Goldman, Interference effects in the relaxation of a pair of unlike spin-$\frac{1}{2}$ nuclei, *J. Magn. Reson.* **60,** 437–452 (1984).
2. N. Tjandra, A. Szabo, and A. Bax, Protein backbone dynamics and ^{15}N chemical shift anisotropy from quantitative measurement of relaxation interference effects, *J. Am. Chem. Soc.* **118,** 6986–6991 (1996).
3. N. Tjandra and A. Bax, Solution NMR measurement of amide proton chemical shift anisotropy in ^{15}N-enriched proteins. Correlation with hydrogen bond length, *J. Am. Chem. Soc.* **119,** 8076–8082 (1997).
4. (a) M. Tessari, F. A. A. Mulder, R. Boelens, and G. W. Vuister, Determination of amide proton CSA in ^{15}N-labeled proteins using ^{1}H CSA/^{15}N–^{1}H dipolar and ^{15}N CSA/^{15}N–^{1}H dipolar cross-correlation rates, *J. Mag. Reson.* **127,** 128–133 (1997); (b) M. Tessari, H. Vis, R. Boelens, R. Kaptein, and G. W. Vuister, Quantitative measurement of relaxation interference effects between $^{1}H_N$ CSA and ^{1}H–^{15}N dipolar interaction : Correlation with secondary structure, *J. Am. Chem. Soc.* **119,** 8985–8990 (1997).
5. N. Tjandra and A. Bax, Large variations in $^{13}C^{\alpha}$ chemical shift anisotropy in proteins correlate with secondary structure, *J. Am. Chem. Soc.* **119,** 9576–9577 (1997).
6. S. Ando, I. Ando, A. Shoji, and T. Ozaki, Intermolecular hydrogen-bonding effect on ^{13}C NMR chemical shifts of glycine residue carbonyl carbons of peptides in the solid state, *J. Am. Chem. Soc.* **110,** 3380–3386 (1988).
7. Z. Gu and A. McDermott, Chemical shielding anisotropy of protonated and deprotonated carboxylates, *J. Am. Chem. Soc.* **115,** 4282–4285 (1993).
8. Z. Gu, R. Zambrano and A. McDermott, Hydrogen bonding of carboxyl groups in solid-state amino acids and peptides: Comparison of carbon chemical shielding, infrared frequencies and structures, *J. Am. Chem. Soc.* **116,** 6368–6372 (1994).
9. Z. Gu, C. F. Ridenour, C. E. Bronnimann, T. Iwashita, and A. McDermott, Hydrogen bonding and distance studies of amino acids and peptides using solid-state 2D ^{1}H–^{13}C heteronuclear correlation spectroscopy, *J. Am. Chem. Soc.* **118,** 822–829 (1996).
10. A. C. de Dios and E. Oldfield, Chemical shifts of carbonyl carbons in peptides and proteins, *J. Am. Chem. Soc.* **116,** 11485–11488.
11. J. Engelke and H. Rüterjans, Backbone dynamics of proteins derived from carbonyl carbon relaxation times at 500, 600 and 800 MHz: Application to ribonuclease T1, *J. Biomolec. NMR* **9,** 63–78 (1997).
12. P. Allard and T. Härd, NMR relaxation mechanisms for backbone carbonyl carbons in a ^{13}C, ^{15}N-labeled protein, *J. Magn. Reson.* **126,** 48–57 (1997).
13. K. T. Dayie and G. Wagner, Carbonyl carbon probe of local mobility in ^{13}C, ^{15}N-enriched proteins using high-resolution nuclear magnetic resonance, *J. Am. Chem. Soc.* **119,** 7797–7806 (1997).
14. F. Cordier, B. Brutscher and D. Marion, Measurement of $^{13}C^{\alpha}$–^{13}CO Cross-relaxation rates in ^{15}N-/^{13}C-labeled proteins, *J. Biomolec. NMR* **7,** 163–168 (1996).
15. L. Zeng, M. W. F. Fischer, and E. R. P. Zuiderweg, Study of protein

dynamics in solution by measurement of $^{13}C^{\alpha}$–^{13}CO NOE and ^{13}CO longitudinal relaxation, *J. Biomolec. NMR* **7,** 157–162 (1996).

16. D. E. Woessner, Nuclear spin relaxation in ellipsoids undergoing rotational Brownian motion, *J. Chem. Phys.* **17,** 647–654 (1962).
17. (a) G. Lipari and A. Szabo, Model-free approach to the interpretation of nuclear magnetic relaxation in macromolecules. 1. Theory and range of validity, *J. Am. Chem. Soc.* **104,** 4546–4558 (1982); (b) G. Lipari and A. Szabo, Model-free approach to the interpretation of nuclear magnetic relaxation in macromolecules. 2. Analysis of experimental results, *J. Am. Chem. Soc.* **104,** 4559–4570 (1982).
18. J. Chung, E. Oldfield, A. Thevand, and L. Werbelow, A "magic-angle" sample-spinning nuclear magnetic resonance spectroscopy study of interference effects in nuclear spin relaxation of polymers, *J. Magn. Reson.* **100,** 69–81 (1992).
19. M. W. Fischer, L. Zeng, Y. Pang, W. Hu, A. Majumdar, and E. R. P. Zuiderweg, Experimental characterization of models for backbone pico-second dynamics in proteins. Quantification of NMR auto- and cross correlation relaxation mechanisms involving different nuclei of the peptide plane, *J. Am. Chem. Soc.* **119,** 12629–12642 (1997).
20. G. Bodenhausen and R. R. Ernst, The accordion experiment, a simple approach to three-dimensional NMR spectroscopy, *J. Magn. Reson.* **45,** 367–373 (1981).
21. G. Bodenhausen and R. R. Ernst, Direct determination of rate constants of slow dynamic processes by two-dimensional "accordion" spectroscopy in nuclear magnetic resonance, *J. Am. Chem. Soc.* **104,** 1304–1309 (1982).
22. L. E. Kay and J. H. Prestegard, Spin–lattice relaxation rates of coupled spins from 2D accordion spectroscopy, *J. Magn. Reson.* **77,** 599–605 (1988).
23. A. M. Mandel and A. G. Palmer III, Measurement of relaxation-rate constants using constant-time accordion NMR spectroscopy, *J. Magn. Reson. A* **110,** 62–72 (1994).
24. D. Marion, M. Ikura, R. Tschudin, and A. Bax, Rapid recording of 2D NMR spectra without phase cycling. Application to the study of hydrogen exchange in proteins, *J. Magn. Reson.* **85,** 393–399 (1989).
25. L. E. Kay, M. Ikura, R. Tschudin, and A. Bax, Three-dimensional triple-resonance NMR spectroscopy of isotopically enriched proteins, *J. Magn. Reson.* **89,** 496–514 (1990).
26. I. Burghardt, R. Konrat, and G. Bodenhausen, Measurement of cross-correlation of fluctuations of dipolar couplings and anisotropic chemical shifts by selective spin locking, *Molec. Phys.* **75,** 467–486 (1992).
27. K. Peruvshin, R. Riek, G. Wider, and K. Wüthrich, Attenuated T_2 relaxation by mutual cancellation of dipole–dipole coupling and chemical shift anisotropy indicates an avenue to NMR structures of very large biological macromolecules in solution, *Proc. Natl. Acad. Sci. USA* **94,** 12366–12371 (1997).
28. R. B. Hill, J. M. Flanagan, and J. H. Prestegard, ^{1}H and ^{15}N NMR assignments, secondary structure and tertiary fold of *E. coli* DnaJ(1–78), *Biochemistry* **34,** 5587–5596 (1995).
29. K. Huang, J. M. Flanagan, and J. H. Prestegard, The influence of C-terminal extension on the structure of the "J-domain" in *E. coli* DnaJ, *Protein Sci.,* in press.
30. P. T. Boggs, R. H. Byrd, T. E. Rogers, and R. B. Schnabel, "User's Reference Guide for ODRPACK 2.01—Software for Weighted Orthogonal Distance Regression," NIST IR4834, U. S. Government Printing Office (1992).
31. M. Andrec and J. H. Prestegard, A metropolis Monte Carlo implementation of Bayesian time-domain parameter estimation: Application to coupling constant estimation from antiphase multiplets, *J. Magn. Reson.* **130,** 217–232 (1998).
32. I. Najfeld, K. T. Dayie, G. Wagner, and T. F. Havel, A robust method for estimating cross-relaxation rates from simultaneous fits to build-up and decay curves, *J. Magn. Reson.* **124,** 372–382 (1997).
33. T. G. Oas, C. J. Hartzell, F. W. Dahlquist, and G. P. Drobny, Determination of the ^{15}N and ^{13}C chemical shift tensors of L-[^{13}C] alanyl-L-[^{15}N] alanine from the dipole-coupled patterns, *J. Am. Chem. Soc.* **109,** 5962–5966 (1987).
34. M. D. Lumsden, R. E. Wasylishen, K. Eichele, M. Schindler, G. H. Penner, W. P. Power, and R. D. Curtis, Carbonyl carbon and nitrogen chemical shift tensors of the amide fragment of acetamide and *N*-methylacetamide, *J. Am. Chem. Soc.* **116,** 1403–1413 (1994).
35. Y. Hiyama, C. H. Niu, J. V. Silverton, A. Bavoso, and D. A. Torchia, Determination of ^{15}N chemical shift tensor via ^{15}N–^{2}H dipolar coupling in Boc-glycylglycyl[^{15}N] glycine benzyl ester, *J. Am. Chem. Soc.* **110,** 2378–2383 (1988)
36. A. Palmer III, N. J. Skelton, W. J. Chazin, P. E. Wright, and M. Rance, Supression of the effects of cross-correlation between dipolar and anisotropic chemical shift relaxation mechanisms in the measurement of spin–spin relaxation rates, *Molec. Phys.* **75,** 699–711 (1992).
37. A. Szabo, Theory of fluorescence depolarization in macromolecules and membranes, *J. Chem. Phys.* **81,** 150–167, (1984).
38. V. A. Daragan and K. H. Mayo, Motional model analyses of protein and peptide dynamics using ^{13}C and ^{15}N relaxation, *Prog. NMR Spectrosc.* **31,** 63–105 (1997).
39. R. N. Zare, "Angular Momentum. Understanding Spatial Aspects in Chemistry and Physics," Wiley–Interscience, New York (1988).